

PLURIPOTENT STEM CELLS

Pluripotent stem cell-based screening identifies CUDC-907 as an effective compound for restoring the in vitro phenotype of Nakajo-Nishimura syndrome

Naoya Kase¹ | Madoka Terashima¹ | Akira Ohta² | Akira Niwa¹  |
 Fumiko Honda-Ozaki^{1,3} | Yuri Kawasaki¹ | Tatsutoshi Nakahata² |
 Nobuo Kanazawa⁴ | Megumu K. Saito¹ 

¹Department of Clinical Application, Center for iPS Cell Research and Application (CiRA), Kyoto University, Kyoto, Japan

²Department of Fundamental Cell Technology, Center for iPS Cell Research and Application (CiRA), Kyoto University, Kyoto, Japan

³Department of Pediatrics and Developmental Biology, Graduate School of Medical and Dental Sciences, Tokyo Medical and Dental University, Tokyo, Japan

⁴Department of Dermatology, Wakayama Medical University, Wakayama, Japan

Correspondence

Megumu K. Saito, MD, PhD, Department of Clinical Application, Center for iPS Cell Research and Application (CiRA), Kyoto University, Kyoto 6068507, Japan.
 Email: msaito@cira.kyoto-u.ac.jp

Funding information

Wakayama Medical University Special Grant-in-Aid for Research Projects; Translational Research program; Strategic PRomotion for practical application of INnovative medical Technology (TR-SPRINT) from AMED; Practical Research Project for Rare/Intractable Diseases from AMED, Grant/Award Number: 17929899; Acceleration Program for Intractable Diseases Research, Grant/Award Numbers: 15652070, 17935244; Japan Agency for Medical Research and Development (AMED)

Abstract

Nakajo-Nishimura syndrome (NNS) is an autoinflammatory disorder caused by a homozygous mutations in the *PSMB8* gene. The administration of systemic corticosteroids is partially effective, but continuous treatment causes severe side effects. We previously established a pluripotent stem cell (PSC)-derived NNS disease model that reproduces several inflammatory phenotypes, including the overproduction of monocyte chemoattractant protein-1 (MCP-1) and interferon gamma-induced protein-10 (IP-10). Here we performed high-throughput compound screening (HTS) using this PSC-derived NNS model to find potential therapeutic candidates and identified CUDC-907 as an effective inhibitor of the release of MCP-1 and IP-10. Short-term treatment of CUDC-907 did not induce cell death within therapeutic concentrations and was also effective on primary patient cells. Further analysis indicated that the inhibitory effect was post-transcriptional. These findings suggest that HTS with PSC-derived disease models is useful for finding drug candidates for autoinflammatory diseases.

KEYWORDS

chemokines, hereditary autoinflammatory diseases, high-throughput screening assays, histone deacetylase inhibitors, LMP7 protein, pluripotent stem cells

1 | INTRODUCTION

Proteasome-associated autoinflammatory syndromes (PRAAS) are a recently defined group of autoinflammatory disorders caused by the

mutations of proteasome subunits or their assembly factors.¹ PRAAS include diseases such as chronic atypical neutrophilic dermatosis with lipodystrophy and elevated temperature (CANDLE),² POMP-related auto-inflammation and immune dysregulation disease (PRAID),³ and

This is an open access article under the terms of the Creative Commons Attribution-NonCommercial License, which permits use, distribution and reproduction in any medium, provided the original work is properly cited and is not used for commercial purposes.

© 2020 The Authors. STEM CELLS TRANSLATIONAL MEDICINE published by Wiley Periodicals LLC on behalf of AlphaMed Press.

Nakajo-Nishimura syndrome (NNS). NNS is caused by a homozygous mutation in *proteasome subunit beta 8 (PSMB8)/LMP-7* gene.^{4,5} The onset of NNS begins in early infancy with patients showing a pernio-like rash, then developing periodic high fever, and eventually lipomuscular atrophy and joint contractures mainly in the upper body. The administration of systemic corticosteroids is partially effective against symptoms such as the rash and fever, but not the other symptoms. Furthermore, because the constitutive administration of steroids causes severe side effects, the prognosis of NNS patients relatively remains poor.⁶⁻⁹

The proteasome is a highly efficient enzyme complex and essential for the degradation of damaged or unnecessary proteins.¹⁰ Such proteins are mainly degraded by a constitutively expressed proteasome to maintain cellular homeostasis or elude cell stress.¹¹ On the other hand, the immunoproteasome is upregulated upon stimulation by tumor necrosis factor alpha (TNF- α) and/or interferon gamma (IFN- γ), especially in immune cells. The immunoproteasome is required for processing endogenous peptides that are presented on the cell surface as antigens^{11,12} and consists of three types of proteases: β 1i, β 2i, and β 5i. β 5i is encoded by *PSMB8* gene.¹³

Almost all NNS patients have the homozygous c.602G > T mutation in *PSMB8* gene, which causes a G201V amino acid substitution in the β 5i subunit.⁴ It is previously reported that impaired immunoproteasome activity by this mutation causes an excessive accumulation of ubiquitinated and oxidized proteins and an elevated serum concentration of the pro-inflammatory cytokines and chemokines interleukin-6 (IL-6), monocyte chemoattractant protein-1 (MCP-1), and interferon gamma-induced protein-10 (IP-10).⁴ To investigate the detailed pathophysiology of NNS, we previously established isogenic pairs (wild type and mutant *PSMB8* G201) of human pluripotent stem cells (PSCs) with or without the NNS-associated *PSMB8* mutation.¹⁴ We then established an in vitro disease model by establishing immortalized myeloid cell lines (MLs) from PSC-derived monocytic cells.¹⁵ Although this model shows an excessive accumulation of ubiquitinated proteins and increased secretion of IL-6, MCP-1 and IP-10, the definitive pathogenic mechanism is unknown.¹⁴

High-throughput compound screening (HTS) has been widely adopted as a strategy of drug discovery for intractable diseases including autoimmune disorders.¹⁶ HTS combined with PSC-derived disease models has provided novel drug candidates for several diseases including amyotrophic lateral sclerosis, fibrodysplasia ossificans progressiva, and dysferlinopathy.¹⁷⁻¹⁹ Here we established an HTS system using the PSC-derived MLs as model of NNS (NNS-MLs) to discover effective therapeutic candidates for the disease. The HTS system was optimized to identify small molecule compounds inhibiting the production of MCP-1 and IP-10 from NNS-MLs. We thus identified CUDC-907, a histone deacetylase and PI3K-Akt dual inhibitor,²⁰ as the most potent candidate. CUDC-907 seemingly inhibited the translation of MCP-1 and IP-10, thereby decreasing the secretion of these chemokines. These findings suggest that HTS with PSC-derived disease models is an effective approach for identifying therapeutic candidates for PRAAS.

Significance statement

This study identified a histone deacetylase inhibitor CUDC-907 as a potential effective compound for ameliorating overproduction of inflammatory chemokines in an autoinflammatory disease, Nakajo-Nishimura syndrome. High-throughput screening performed using pluripotent stem cell-derived monocytic cell lines. Data from this study prove the validity of the screening system as a versatile platform for seeking candidate compounds for the treatment of congenital immunological disorders associated with monocytic lineage cells.

2 | MATERIAL AND METHODS

2.1 | Ethics

This study was approved by the Ethics Committees of Kyoto University (R0091/G0259) and Wakayama Medical University. Written informed consent was obtained from the patients or their guardians in accordance with the Declaration of Helsinki. The use of human embryonic stem cells (ESCs) was approved by the Ministry of Education, Culture, Sports, Science and Technology (MEXT) of Japan.

2.2 | Cell culture

Fibroblasts were collected from two healthy donors (Healthy #1, Healthy #2) and two patients (NNS #1, NNS #2). These fibroblasts were cultured in Dulbecco's modified eagle medium (08459-64; Nacalai Tesque) in the presence of 10% fetal calf serum (F0926; Sigma-Aldrich) and passaged via dissociation into single cells using 0.25% Trypsin-EDTA (25200-072; Gibco). For the chemokine and cytotoxicity assays, the fibroblasts were stimulated with 10 ng/mL TNF- α (210-TA; R&D Systems) and 10 ng/mL IFN- γ (285-IF; R&D Systems) for 72 hours to induce the immunoproteasome before the experiments. For the cell growth curve analysis, the fibroblasts were not stimulated.

Induced pluripotent stem cells (iPSCs) were established from the fibroblasts of NNS#1.¹⁴ MLs were previously established from iPSCs bearing mutant (G201V) homozygous *PSMB8* (MT-iPS-MLs), their isogenic wild-type counterpart (WT-iPS-MLs), and from KhES1 ESCs bearing the same *PSMB8* mutation (MT-ES-MLs).¹⁴ In brief, the knockin or repair of mutant *PSMB8* was made by the CRISPR-Cas9 (D10A) double nicking system. PSCs dissociated into single cells were transfected with the single-guide RNA vector and Cas9 vector by an NEPA21 electroporator (Nepagene). Monocyte differentiation was performed according to previously described protocols with some modifications²¹ (Figure S1). To establish the MLs, differentiated monocytes were transfected with a lentiviral vector encoding *BMI1*, *cMYC*, and *MDM2*.¹⁵ The MLs were cultured

TABLE 1 The source of compounds in the HTS

Enzo-FDA (FDA-approved drugs)	Fixed	636
ENZO ICCB (worldwide drugs)	Fixed	477
Microsource-US drugs (FDA-approved drugs)	Fixed	1020
Microsource-international drugs (worldwide drugs)	Fixed	238
Sigma LOPAC	Fixed	1280
Kinase inhibitor Cell-permeable compounds	CiRA special selection	1254
Bioactive compounds	CiRA special selection	916
	Total	5821

Abbreviation: HTS, high-throughput compound screening.

in StemPro-34 serum-free medium (10639-011; Gibco) containing 2 mM L-glutamine (25030-081; Gibco) in the presence of 50 ng/mL macrophage colony stimulating factor (M-CSF) (216-MC; R&D Systems) and 50 ng/mL granulocyte macrophage colony stimulating factor (GM-CSF) (215-GM; R&D Systems). KhES1 ESCs were kindly provided by Dr Hirofumi Suemori (Kyoto University, Kyoto, Japan).

2.3 | HTS system

We used MT-iPS-MLs and homogeneous time-resolved fluorescence-based chemokine measurements for the HTS system. The compound library is described in Table 1. For the first and second screenings, 5×10^3 MT-iPS-MLs were seeded into each well of 384-well plates. The plates were individually prepared for the detection of MCP-1 or IP-10. The cells were treated with compounds at concentrations of 1 μ M (first screening) and 100 nM (second screening). Three hours later, 50 ng/mL lipopolysaccharide (LPS) (tlrl-pek1ps; InvivoGen) for MCP-1 and 100 ng/mL IFN- γ for IP-10 was added for the stimulation. After the subsequent culture for 21 hours, the supernatants were sampled, and the Human CCL2 (MCP-1) Kit (62HCCL2PEG; Cisbio) or Human CXCL10 (IP-10) Kit (62HCX10PEG; Cisbio) was added to detect MCP-1 or IP-10 (Figure 1A). The chemokine concentration was detected by using POWERSCAN4 (DS Pharma Biomedical). The inhibition efficiency of each compound was determined by the following formula.

$$\% \text{ inhibition} = \frac{[\text{DMSO}] - [\text{Comp.}]}{[\text{DMSO}] - [\text{UT}]} \times 100,$$

where [UT], [DMSO], and [Comp.] are the MCP-1 or IP-10 concentration of untreated control, LPS or IFN- γ stimulation with dimethyl sulfoxide (DMSO), and LPS or IFN- γ stimulation with the target compound, respectively. Validation of the hit compounds with MT-ES-MLs was performed using the same procedure as the second screening.

2.4 | Enzyme-linked immunosorbent assay

The concentrations of cytokines and chemokines in MLs and fibroblasts were measured by using a LEGENDplex Human Adipokine Panel (740 196; BioLegend) according to the manufacturer's protocol. Quantification was done with Guava easyCyte (Luminex). After seeding 1×10^4 MLs or 5×10^3 fibroblasts into each well of 96-well plates, the compounds in DMSO (D2650; Sigma-Aldrich) were applied. Three hours later, TNF- α and IFN- γ at 100 ng/mL for the MLs and 10 ng/mL for the fibroblasts were added for the stimulation. After culturing for 21 hours, the supernatants were sampled.

2.5 | Cell cytotoxicity

To evaluate cell cytotoxicity by the extracellular lactate dehydrogenase (LDH) activity, Cytotoxicity Detection Kit^{PLUS} was used according to the manufacturer's protocol (4744934001; Merck). For MT-ES-MLs, 5×10^3 cells were seeded into each well of 384-well plates, and then compounds in DMSO at a concentration of 100 nM were applied. Three hours later, 100 ng/mL IFN- γ was added for the stimulation. After culturing for 21 hours, the supernatants were sampled. Detections were performed by using POWERSCAN4. For MT-iPS-MLs and fibroblasts, 1×10^4 MT-iPS-MLs and 1.5×10^3 NNS#1 fibroblasts were seeded into each well of 96-well plates. After culturing for 24 hours, the supernatants were sampled. Detections were performed by using 2104 EnVision Multilabel Plate Readers (PerkinElmer). In every case, total cell lysates (100% cell death) from the same number of cells were used as the positive control.

To evaluate cell viability by the intracellular nicotinamide adenine dinucleotide (NADH) activity, 5×10^4 MT-iPS-MLs or 5×10^3 NNS#1 fibroblasts were seeded into each well of 96-well plates. After culturing for 24 hours, Cell Counting Kit-8 (CK04; Dojindo) was used according to the manufacturer's protocol.

2.6 | RNA isolation and quantitative polymerase chain reaction

Total RNA was column-purified with the RNeasy Mini Kit (74 106; Qiagen) and treated with RNase-free DNase (79 254; Qiagen). Purified RNA was reverse transcribed using PrimeScript RT Master Mix (RR037A; Takara) according to the manufacturer's protocol. Quantitative polymerase chain reaction was performed using StepOnePlus (Applied Biosystems) with TB Green Premix Ex Taq II (RR820A; Takara). The primer sequences used in this study are listed in Table 2.

2.7 | Immunoblotting

A total of 3×10^5 cells were lysed for 30 minutes on ice in RIPA buffer (188-02453; Wako) with protease inhibitor cocktail (04080-11; Nacalai Tesque). After being centrifuged at 15 000g for 5 minutes at

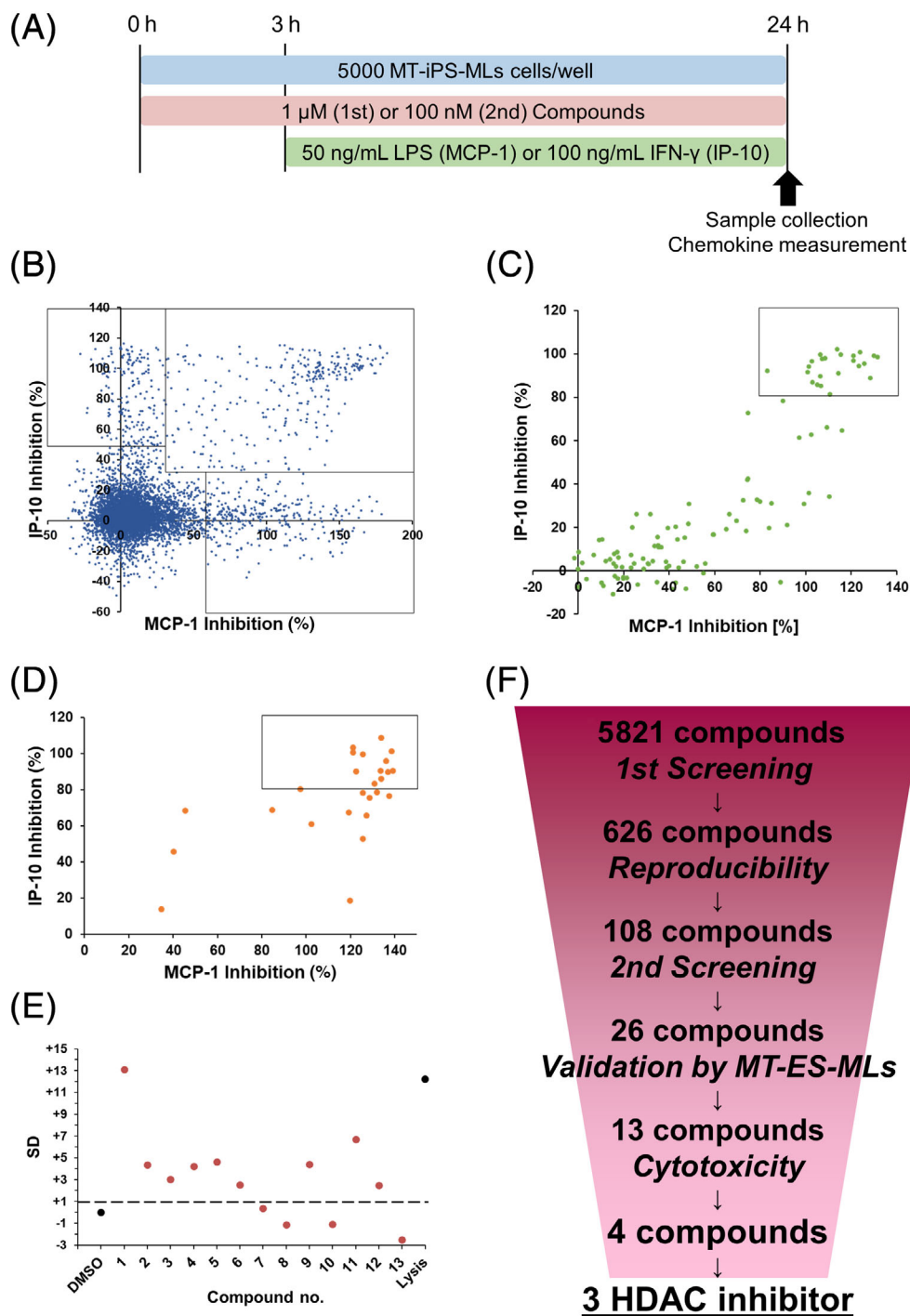


FIGURE 1 Results of the HTS. A, Schematic representation of the time course and culture condition for the sampling. B, C, Results of the first (B) and second (C) screening using MT-iPS-MLs. D, Validation of the hit compounds using MT-ES-MLs. B-D, Plots inside the squares shows hit compounds. E, Results of the cytotoxic evaluation. Compounds below the dotted line are considered hits. DMSO and lysis (100% cell death) are plotted as controls. F, Schematic representation of the HTS results. HTS, high-throughput compound screening

Gene	Forward	Reverse
CCL2	5' GCCAGATGCAATCAATGCC	5' TCTTGAAGATCACAGCTTCTTTGG
CXCL10	5' AAGTGGCATTCAAGGAGTACCT	5' ACACGTGGACAAAATTGGCT
GAPDH	5' GAGAAGGCTGGGGCTCAT	5' TGCTGATGATCTTGAGGCTG

TABLE 2 The list of primers for the quantitative polymerase chain reaction

4°C, the supernatants were collected. The total amount of proteins in the lysates was quantified by the DC Protein Assay (500-0116JA; Bio-Rad) and 2104 EnVision Multilabel Plate Readers (PerkinElmer) according to the manufacturer's protocol, and the lysates were

adjusted to the same concentrations. The lysates were boiled for 5 minutes in 4x Laemmli Sample Buffer (161-0747; Bio-Rad) containing 2-Mercaptoethanol (21418-42; Nacalai Tesque). The proteins were then separated by sodium dodecyl sulfate-polyacrylamide

gel electrophoresis and transferred onto an Immobilon-P membrane (IPVH00010; Merck). The membranes were blocked with 10% nonfat milk (190-12 865; Wako) in Tris-buffered saline plus 0.1% Tween20 (9005-64-5; Sigma-Aldrich) and reacted with the indicated antibodies. The antibodies used for immunoblotting were as follows: monoclonal anti-GAPDH antibody (2118, CST), polyclonal anti-MCP-1 antibody (ab9669, Abcam), polyclonal anti-IP-10 antibody (ab8098, Abcam), horseradish peroxidase (HRP)-conjugated anti-rabbit IgG antibody (7074, CST), and HRP-conjugated anti-mouse IgG antibody (7076, CST). SuperSignal West Femto Maximum Sensitivity Substrate (34 095; Thermo Fisher) was used for the chemiluminescence. Images were obtained using ImageQuant LAS 4000 (GE Healthcare).

2.8 | Cell growth curves

To determine cell growth, 5×10^3 fibroblasts were seeded into each well of six-well plates. The culture medium was changed every 3 days. After cell seeding, unstained cells were counted every 3 days by using trypan blue.

2.9 | Statistics

All statistical analyses and IC_{50} values were performed using GraphPad Prism (GraphPad Software). Statistical methods are described in the figure legends.

3 | RESULTS

3.1 | HTS identifies HDAC inhibitors as therapeutic candidates for NNS

We performed HTS to identify drug candidates for NNS. Compounds were evaluated by the inhibition rates of MCP-1 and IP-10, both of which are pro-inflammatory chemokines specifically elevated in NNS patients.^{4,14} Although IL-6 is also specifically elevated in NNS patients, blockage of the IL-6 receptor by the administration of the anti-IL-6 receptor tocilizumab provided limited therapeutic effects.²² Therefore, we focused on suppressing both MCP-1 and IP-10. The compounds library consisted of 5821 compounds including approved drugs, kinase inhibitors, and bio-active chemicals (Table 1). The cells were pretreated with compounds for 3 hours and treated subsequently with LPS or IFN- γ to induce MCP-1 or IP-10, respectively (Figure 1A). In the first and second screenings, we used MT-iPS-MLs. We first evaluated the effect of the 5821 compounds on MT-iPS-MLs at a concentration of 1 μ M. We defined the criteria for hit compounds as >60% inhibition of MCP-1, >50% inhibition of IP-10, or >30% inhibition of both (Figure 1B). To confirm the reproducibility, we evaluated 626 hit compounds of the first screening following the same

protocol. We defined the criteria for hit compounds as >70% inhibition of MCP-1 and >30% inhibition of IP-10 (Figure S2). We excluded several hit compounds from the results because of their potential cytotoxicity. In the second screening, we evaluated 108 compounds at a concentration of 100 nM and picked up those with >80% inhibition of both MCP-1 and IP-10. The second screening yielded 26 hit compounds (Figure 1C). To validate the reproducibility of the results, we evaluated the inhibitory effects of the 26 compounds on another clone, MT-ES-MLs, at the same 100 nM concentration. We thus obtained 13 hit compounds that inhibited the secretion of both MCP-1 and IP-10 at more than 80% (Figure 1D). Finally, we evaluated the cytotoxicity of these 13 compounds on MT-ES-MLs at the same concentration. Four compounds showed an LDH release less than 1 SD from the mean of DMSO control and were considered nontoxic (Figure 1E). Since three of the four compounds are HDAC inhibitors, we conducted detailed comparative studies on these three (Figure 1F).

3.2 | CUDC-907 inhibits MCP-1 and IP-10 production at a lower concentration

We next compared the inhibitory effects of the three HDAC inhibitors: CUDC-907 (Figure 2A),²⁰ JNJ-26481585 (Figure 2B),²³ and LAQ824 (Figure 2C).²⁴ The 50% inhibitory concentration (IC_{50}) values were calculated from the dose-dependent effects on MT-iPS-MLs (Figure 2D-I). Among the three compounds, CUDC-907 showed the lowest IC_{50} for both MCP-1 and IP-10 secretion (Table 3). We therefore focused on CUDC-907 as the first choice for NNS. CUDC-907 is known to be a dual inhibitor of HDAC and PI3K-Akt and is an effective therapeutic candidate for acute myeloid leukemia, in which the PI3K-Akt pathway is constitutively activated.²⁵ However, there are no reports yet on its effect on the production of pro-inflammatory cytokines or chemokines. Since HDAC inhibitors are widely known to arrest the cell cycle,²⁶ we measured the effect of CUDC-907 on cell cytotoxicity by detecting intracellular NADH and extracellular LDH activities. Although CUDC-907 treatment slightly decreased the viability of MT-iPS-MLs in a dose-dependent manner, almost no cytotoxicity was observed within effective concentrations (Figures 2J,K and S3A,B). These results suggest that CUDC-907 avoids serious cytotoxic side effects within the effective window and that its inhibitory effect is not attributed to the consequence of cell death.

3.3 | CUDC-907 exerts effective inhibition in patient fibroblasts

To address the consistency of the inhibitory effects of CUDC-907 on other cell types, we next used primary patient fibroblasts. The expression of the immunoproteasome in fibroblasts is lower than in immune cells.²⁷ We therefore measured the production of cytokines after

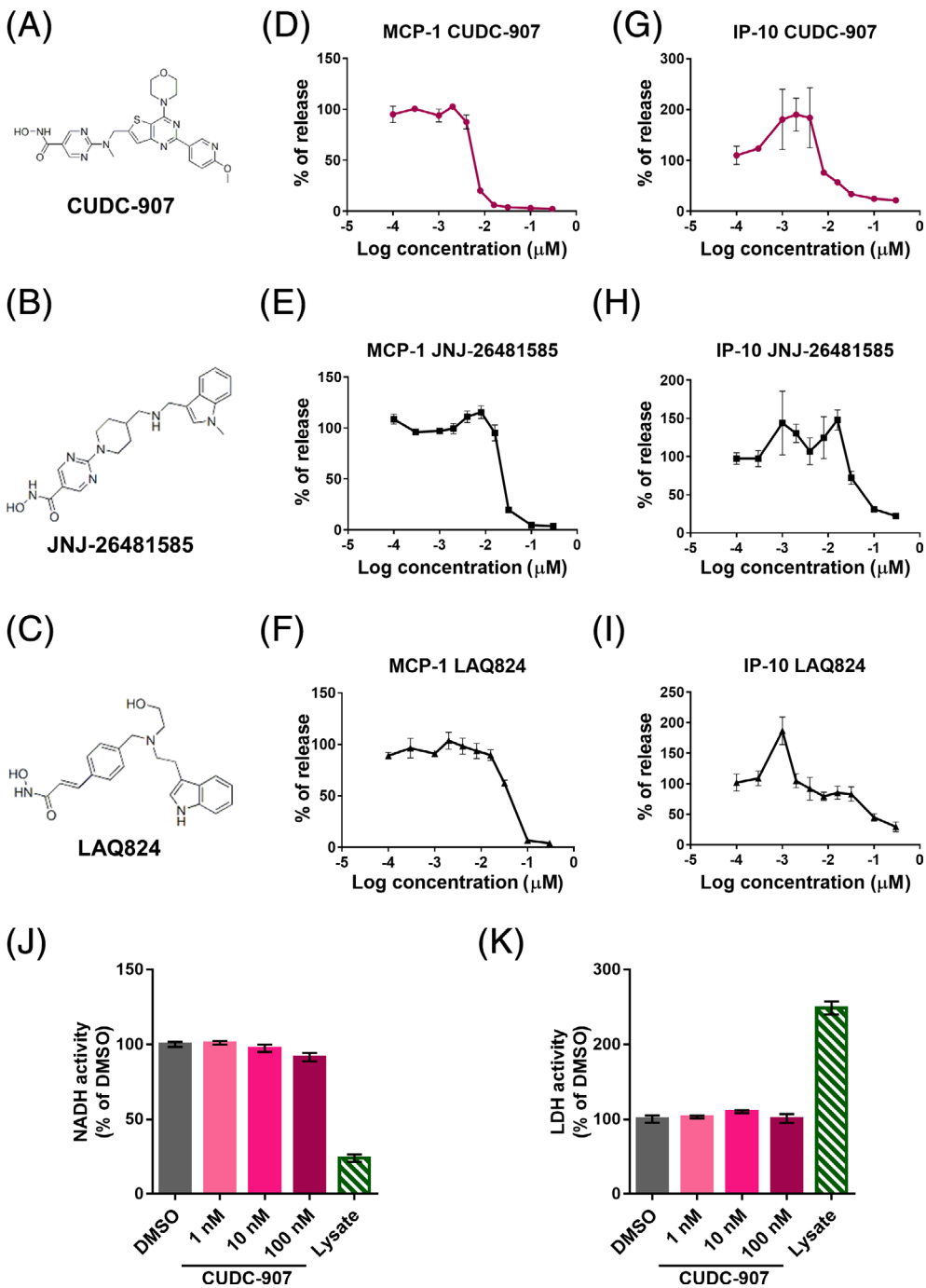


FIGURE 2 Comparison of three HDAC inhibitors. A-C, Structural formula of each compound. D-I, Dose-dependent inhibitory effects of the compounds on MCP-1 (D-F) and IP-10 (G-I) ($n = 3$). J, K, Cell cytotoxicity by detecting intracellular NADH (J) and extracellular LDH activities (K) in the presence of CUDC-907 under the indicated concentrations ($n = 3$). IP-10, interferon gamma-induced protein-10; LDH, lactate dehydrogenase; MCP-1, monocyte chemoattractant protein-1

TABLE 3 IC_{50} values of three HDAC inhibitors

Compound	MCP-1 (nM)	IP-10 (nM)
CUDC-907	6.0	21.7
JNJ-26481585	25.7	73.6
LAQ824	38.6	101.9

Note: IC_{50} values were calculated from the dose-response curves shown in Figure 2D-I.

longer treatment (72 hours) with TNF- α and IFN- γ to induce the immunoproteasome sufficiently to show the phenotype of NNS

(Figure 3A). Since the amount of secreted IP-10 was very small in fibroblasts, we could not compare fibroblasts from patients and healthy donors (data not shown). However, the secretion of MCP-1 from patient fibroblasts (NNS #1, NNS #2) was significantly higher than that from healthy donor-derived fibroblasts (Healthy #1, Healthy #2) (Figure 3B). The IC_{50} of CUDC-907 on the inhibition of MCP-1 secretion was comparable to that in MT-iPS-MLs (Figure 3C). Furthermore, we measured the cytotoxicity on patient fibroblasts. Almost no cytotoxicity was observed within the effective concentrations (Figure 3D,E and S3C,D). Therefore, CUDC-907 inhibits the secretion of MCP-1 in patient fibroblasts at similar concentrations as in MT-iPS-MLs without cell death.

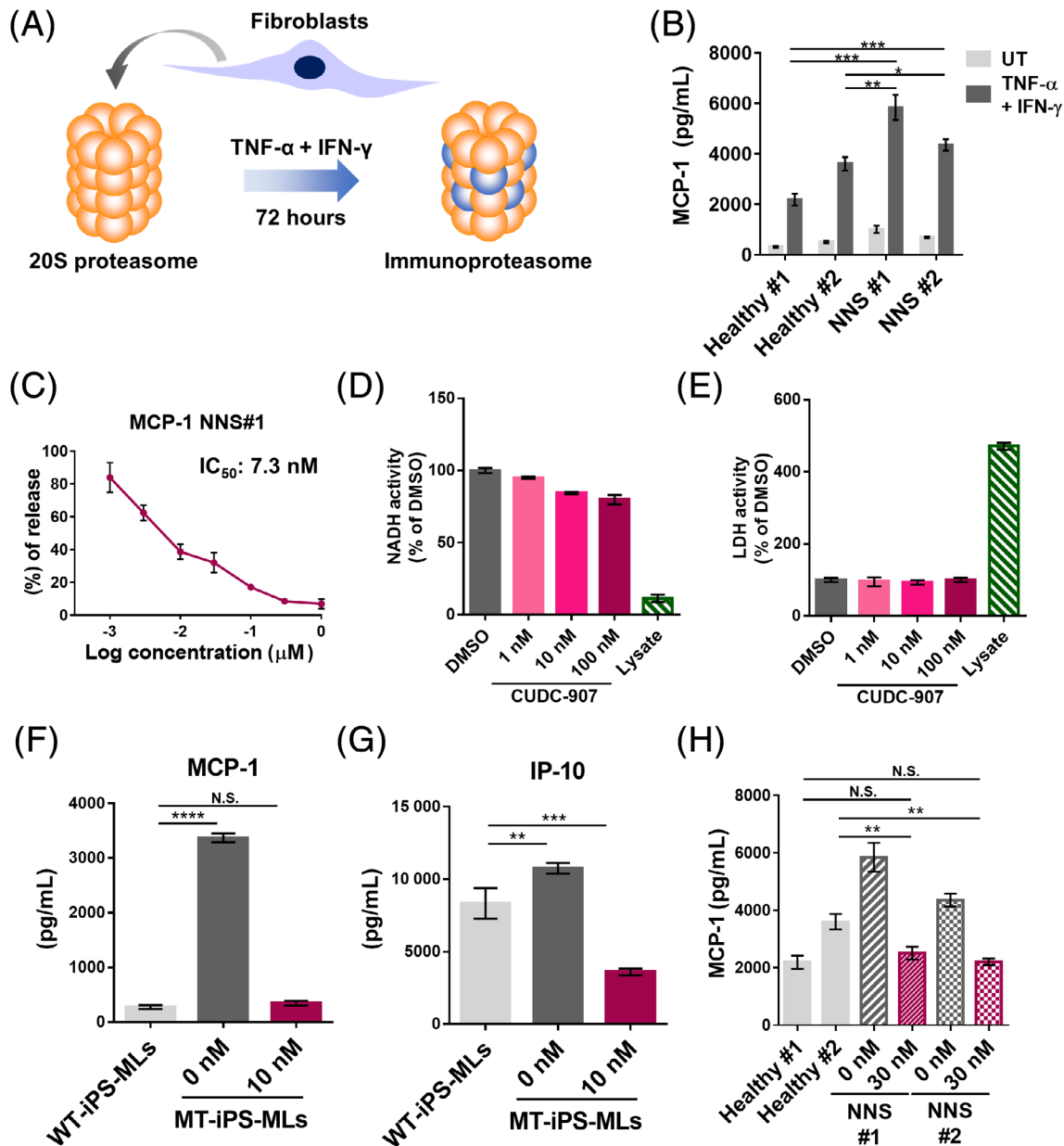


FIGURE 3 Effects of CUDC-907 on primary patient fibroblasts. A, Schematic representation of the immunoproteasome induction in fibroblasts. B, MCP-1 secreted from fibroblasts under TNF- α and IFN- γ treatment (n = 3). Statistical analysis was performed by Student's t test: * $P < .05$; ** $P < .01$; *** $P < .005$. C, Dose-dependent inhibitory effects of CUDC-907 on MCP-1 in NNS #1 fibroblasts. D, E, Cell cytotoxicity of NNS #1 fibroblasts by detecting intracellular NADH (D) and extracellular LDH activities (E) in the presence of CUDC-907 at the indicated concentrations (n = 3). F, G, Secreted MCP-1 (F) and IP-10 (G) from WT-iPS-MLs and MT-iPS-MLs in the presence of CUDC-907 (n = 3). Statistical analysis was performed by one-way analysis of variance with Dunnett's multiple comparison: ** $P < .01$; *** $P < .005$; **** $P < .001$. H, Secreted MCP-1 from fibroblasts in the presence of CUDC-907 (n = 3). Statistical analysis was performed by Student's t test: ** $P < .01$. IFN- γ , interferon gamma; IP-10, interferon gamma-induced protein-10; LDH, lactate dehydrogenase; MCP-1, monocyte chemoattractant protein-1; NNS, Nakajo-Nishimura syndrome; TNF- α , tumor necrosis factor alpha

To investigate the long-term effects of CUDC-907 on cell viability, we next evaluated cell growth under CUDC-907 treatment. The growth of NNS #1 fibroblasts in the presence of CUDC-907 for 2 weeks was inhibited even at very low concentration compared to DMSO control (Figure S4). This finding suggested that long-term exposure to CUDC-907 might affect cell growth, which could prohibit the direct application of CUDC-907 to the clinical situation.

Notably, when we compared the chemokine secretion level of MLs with or without *PSMB8* mutation (MT-iPS-MLs and WT-iPS-MLs, respectively), CUDC-907 sufficiently suppressed the amount of secreted MCP-1 and IP-10 by MT-iPS-MLs to levels comparable with those secreted by WT-iPS-MLs (Figure 3F,G). CUDC-907 also suppressed MCP-1 secretion from mutant fibroblasts to a similar level as wild-type fibroblasts (Figure 3H).

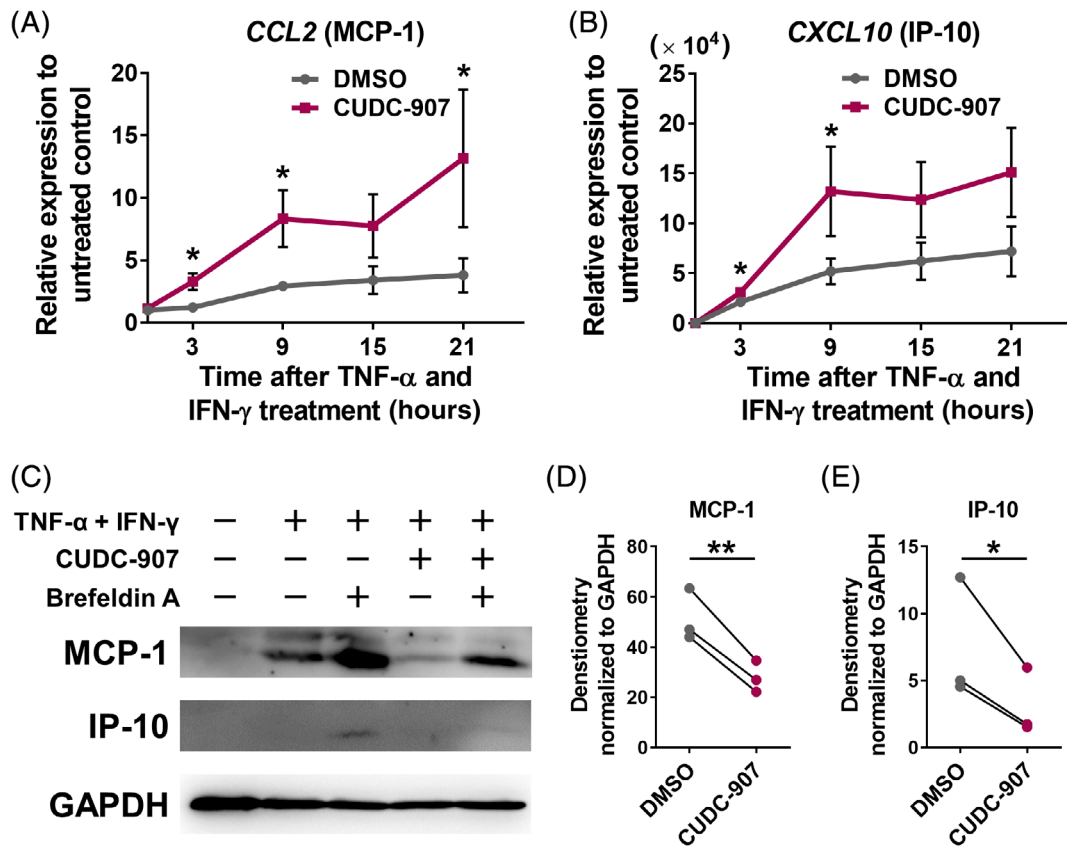


FIGURE 4 Identification of the inhibitory point of CUDC-907. A,B, Relative expression levels of *CCL2* (A) and *CXCL10* (B) genes to dimethyl sulfoxide (DMSO) control ($n = 3$). Cells pretreated with CUDC-907 (10 nM) for 3 hours were sampled after treatment with TNF- α and IFN- γ (100 ng/mL) at the indicated times. The expressions were normalized to the *GAPDH* gene expression. Statistical analysis was performed by Student's *t* test: * $P < .05$. C, Total amount of intracellular MCP-1, IP-10, and glyceraldehyde 3-phosphate dehydrogenase (*GAPDH*) as the loading control. Cells pretreated with CUDC-907 (10 nM) for 30 minutes were sampled after treatment with TNF- α and IFN- γ (100 ng/mL) for 6 hours. Brefeldin A was added 1 hour before the end of the culture. A representative gel image from three independent experiments is shown. D,E, Densitometry of Western blot bands of MCP-1 (D) and IP-10 (E) determined by ImageJ software (National Institutes of Health, Bethesda, Maryland). Statistical analysis was performed by paired *t* test: * $P < .05$; ** $P < .01$. IFN- γ , interferon gamma; IP-10, interferon gamma-induced protein-10; MCP-1, monocyte chemoattractant protein-1; TNF- α , tumor necrosis factor alpha

3.4 | CUDC-907 inhibits the production of MCP-1 and IP-10 post-transcriptionally

To understand the inhibition mechanism of CUDC-907, we quantified the expression levels of *CCL2* gene encoding MCP-1 and *CXCL10* gene encoding IP-10. Contrary to the results of enzyme-linked immunosorbent assay, CUDC-907 upregulated the expression of these two genes (Figure 4A,B), indicating that CUDC-907 exerts its inhibitory effect post-transcriptionally. In line with this assumption, we next observed the protein levels of MCP-1 and IP-10. To detect intracellular MCP-1 and IP-10 levels by Western blot, we inhibited the extracellular release of these cytokines by treating the cells with Brefeldin A, an inhibitor of the protein transportation from the endoplasmic reticulum to the Golgi apparatus.²⁸ In the presence of Brefeldin A, the intracellular levels of MCP-1 and IP-10 were increased in all conditions observed (Figure 4C), indicating Brefeldin A inhibited the extracellular release of MCP-1 and IP-10. In the presence of Brefeldin A, CUDC-907 decreased the intracellular protein levels of MCP-1

and IP-10 (Figure 4C-E). These results indicate that CUDC-907 suppresses the production of MCP-1 and IP-10 by inhibiting translational processes.

4 | DISCUSSION

In this study, we identified an effective compound that restores the disease-associated pro-inflammatory phenotype of NNS by using PSC-based HTS. We used MLs established from PSCs for the HTS, because MLs are easy to propagate, freeze-stock, and differentiate into functional macrophages or dendritic cells.¹⁵ We previously demonstrated that such MLs can be used to model the pro-inflammatory phenotypes of various autoinflammatory disorders.^{14,29-31} Combined with the current study, which successfully identified candidate compounds, we concluded that this ML-based HTS system provides a versatile platform for screening candidate compounds for treating autoinflammatory disorders.

MCP-1 and IP-10 are known as pro-inflammatory chemokines.^{32,33} Their increased production is associated with the

inflammatory symptoms of various diseases, and their suppression sometimes ameliorates the symptoms in diseases such as polycystic kidney disease and rheumatoid arthritis.^{34,35} Therefore, we hypothesized that suppression of the overproduction could alleviate the autoinflammatory symptoms of NNS. However, NNS patients are known to suffer from lipomuscular atrophy in addition to inflammatory symptoms^{6,9}; whether the suppression of MCP-1 and IP-10 also alleviates these atrophic symptoms is unknown. New lipomuscular models of NNS would help in this regard. PSC-derived muscular disease models have contributed to the elucidation of pathophysiologies and drug discovery^{19,36} and should be of benefit to understanding the pathophysiology of the muscular lesions in NNS. The *in vivo* effects of compounds on animal models should be also evaluated.

CUDC-907 is a dual inhibitor of HDAC and PI3K-Akt.²⁰ It has also been reported to inhibit the growth of several tumor cells, including multiple myeloma and chronic lymphoma.^{37,38} Based on those reports, CUDC-907 has been considered an anticancer drug. In this study, we demonstrated for the first time that CUDC-907 has an inhibitory effect on the extracellular release of pro-inflammatory chemokines. This finding suggests that CUDC-907 could be applied to a variety of inflammatory disorders including NNS. However, although short-term cytotoxicity was not identified, CUDC-907 inhibited the cell growth of patient-derived fibroblasts in long-term culture (Figure S4).

Thus, CUDC-907 has two different *in vitro* effects on the cellular phenotype: it inhibits chemokine production with short-term culture and cell growth with long-term culture. The negative effect on cell growth must be overcome before clinical application. Furthermore, the chemokine effect with long-term culture must also be confirmed. Thus, more study of the mechanisms responsible for the inhibition are needed.

A large number of compounds are reported to inhibit the release of extracellular cytokines or chemokines, many of which suppress the expression levels by targeting the inflammatory signaling cascade.^{39,40} However, for some diseases such as asthma and diabetic retinopathy, abnormal post-transcriptional regulation is key.^{41,42} For such diseases, the inhibition of the post-transcriptional phase is considered more appropriate in the therapeutic strategy.^{41,42} In the present study, CUDC-907 was found to inhibit the production of MCP-1 and IP-10 post-transcriptionally. Future study of the detailed molecular mechanism of this effect could provide therapeutic advances for such diseases.

5 | CONCLUSION

In this study, we performed HTS with a PSC-derived NNS disease model to find a potential therapeutic candidate, CUDC-907, which is an HDAC and PI3K-Akt dual inhibitor. CUDC-907 effectively inhibits the release of MCP-1 and IP-10 without inducing cell death and is also effective on primary patient cells. CUDC-907 inhibits the production of MCP-1 and IP-10 post-transcriptionally. These findings suggest that HTS with PSC-derived disease models is an effective approach at identifying therapeutic candidates for autoinflammatory disorders.

ACKNOWLEDGMENTS

We would like to thank Dr Misaki Ouchida for graphical assistance, Ms Harumi Watanabe for providing administrative assistance, and Dr Peter Karagiannis for proofreading the paper. Funding was provided from the Core Center for iPS Cell Research of Research Center Network for Realization of Regenerative Medicine from the Japan Agency for Medical Research and Development (AMED) (M.K.S.), the Acceleration Program for Intractable Diseases Research utilizing Disease-specific iPS cells from AMED (17935244 and 15652070) (M.K.S.), Practical Research Project for Rare/Intractable Diseases from AMED (17929899) (M.K.S.), the Translational Research program; Strategic PRomotion for practical application of INnovative medical Technology (TR-SPRINT) from AMED (M.K.S.), and Wakayama Medical University Special Grant-in-Aid for Research Projects (N.K.).

CONFLICT OF INTEREST

The authors declared no potential conflicts of interest.

AUTHOR CONTRIBUTIONS

N. Kase: conception and design, collection and assembly of data, manuscript writing, data analysis and interpretation; M.K.S.: conception and design, manuscript writing, final approval of manuscript; M.T.: conception and design, collection and assembly of data, data analysis and interpretation; A.O.: conception and design, data analysis and interpretation; A.N., Y.K., F.H.-O., T.N.: conception and design; N. Kanazawa: provision of the study material and patients.

DATA AVAILABILITY STATEMENT

The data that support the findings of this study are available from the corresponding authors upon reasonable request.

ORCID

Akira Niwa  <https://orcid.org/0000-0002-6412-2686>

Megumu K. Saito  <https://orcid.org/0000-0001-8813-3614>

REFERENCES

1. Ebstein F, Poli Harlowe MC, Studencka-Turski M, Krüger E. Contribution of the unfolded protein response (UPR) to the pathogenesis of proteasome-associated autoinflammatory syndromes (PRAAS). *Front Immunol.* 2019;10:2756.
2. Brehm A, Liu Y, Sheikh A, et al. Additive loss-of-function proteasome subunit mutations in CANDLE/PRAAS patients promote type I IFN production. *J Clin Invest.* 2015;125:4196-4211.
3. Poli MC, Ebstein F, Nicholas SK, et al. Heterozygous truncating variants in POMP escape nonsense-mediated decay and cause a unique immune dysregulatory syndrome. *Am J Hum Genet.* 2018;102:1126-1142.
4. Arima K, Kinoshita A, Mishima H, et al. Proteasome assembly defect due to a proteasome subunit beta type 8 (PSMB8) mutation causes the autoinflammatory disorder, Nakajo-Nishimura syndrome. *Proc Natl Acad Sci USA.* 2011;108:14914-14919.
5. Shi X, Xiang X, Wang Z, Ma L, Xu Z. Chinese case of Nakajo-Nishimura syndrome with a novel mutation of the PSMB8 gene. *J Dermatol.* 2019;46:e160-e161.
6. Kanazawa N. Nakajo-Nishimura syndrome: an autoinflammatory disorder showing pernio-like rashes and progressive partial lipodystrophy. *Allergol Int.* 2012;61:197-206.

7. Kunimoto K, Kimura A, Uede K, et al. A new infant case of Nakajo-Nishimura syndrome with a genetic mutation in the immunoproteasome subunit: an overlapping entity with JMP and CANDLE syndrome related to PSMB8 mutations. *Dermatology*. 2013;227:26-30.
8. Ohmura K. Nakajo-Nishimura syndrome and related proteasome-associated autoinflammatory syndromes. *J Inflamm Res*. 2019;12:259-265.
9. Ayaki T, Murata K, Kanazawa N, et al. Myositis with sarcoplasmic inclusions in Nakajo-Nishimura syndrome: a genetic inflammatory myopathy. *Neuropathology and Applied Neurobiology*. 2020. <https://doi.org/10.1111/nan.12614>.
10. Bhattacharyya S, Yu H, Mim C, Matouschek A. Regulated protein turnover: snapshots of the proteasome in action. *Nat Rev Mol Cell Biol*. 2014;15:122-133.
11. Raynes R, Pomatto LC, Davies KJ. Degradation of oxidized proteins by the proteasome: distinguishing between the 20S, 26S, and immunoproteasome proteolytic pathways. *Mol Aspects Med*. 2016;50:41-55.
12. Tanaka K. Role of proteasomes modified by interferon-gamma in antigen processing. *J Leukoc Biol*. 1994;56:571-575.
13. Murata S, Takahama Y, Kasahara M, Tanaka K. The immunoproteasome and thymoproteasome: functions, evolution and human disease. *Nat Immunol*. 2018;19:923-931.
14. Honda-Ozaki F, Terashima M, Niwa A, et al. Pluripotent stem cell model of Nakajo-Nishimura syndrome untangles proinflammatory pathways mediated by oxidative stress. *Stem Cell Reports*. 2018;10:1835-1850.
15. Haruta M, Tomita Y, Imamura Y, et al. Generation of a large number of functional dendritic cells from human monocytes expanded by forced expression of cMYC plus BMI1. *Hum Immunol*. 2013;74:1400-1408.
16. Vincent J, Adura C, Gao P, et al. Small molecule inhibition of cGAS reduces interferon expression in primary macrophages from autoimmune mice. *Nat Commun*. 2017;8:750.
17. Imamura K, Izumi Y, Watanabe A, et al. The Src/c-Abl pathway is a potential therapeutic target in amyotrophic lateral sclerosis. *Sci Transl Med*. 2017;9:eaaf3962.
18. Hino K, Horigome K, Nishio M, et al. Activin-a enhances mTOR signaling to promote aberrant chondrogenesis in fibrodysplasia ossificans progressiva. *J Clin Invest*. 2017;127:3339-3352.
19. Kokubu Y, Nagino T, Sasa K, et al. Phenotypic drug screening for dysferlinopathy using patient-derived induced pluripotent stem cells. *STEM CELLS TRANSLATIONAL MEDICINE*. 2019;8:1017-1029.
20. Qian C, Lai CJ, Bao R, et al. Cancer network disruption by a single molecule inhibitor targeting both histone deacetylase activity and phosphatidylinositol 3-kinase signaling. *Clin Cancer Res*. 2012;18:4104-4113.
21. Yanagimachi MD, Niwa A, Tanaka T, et al. Robust and highly-efficient differentiation of functional monocytic cells from human pluripotent stem cells under serum- and feeder cell-free conditions. *PLoS One*. 2013;8:e59243.
22. Inaba Y, Kunimoto K, Kanazawa N, et al. Effects of a humanized anti-human IL-6 receptor monoclonal antibody on Nakajo-Nishimura syndrome. *Trends Immunother*. 2018;2.
23. Deleu S, Lemaire M, Arts J, et al. The effects of JNJ-26481585, a novel hydroxamate-based histone deacetylase inhibitor, on the development of multiple myeloma in the 5T2MM and 5T33MM murine models. *Leukemia*. 2009;23:1894-1903.
24. Catley L, Weisberg E, Tai YT, et al. NVP-LAQ824 is a potent novel histone deacetylase inhibitor with significant activity against multiple myeloma. *Blood*. 2003;102:2615-2622.
25. Li X, Su Y, Madlambayan G, et al. Antileukemic activity and mechanism of action of the novel PI3K and histone deacetylase dual inhibitor CUDC-907 in acute myeloid leukemia. *Haematologica*. 2019;104:2225-2240.
26. Eckschlager T, Plch J, Stiborova M, et al. Histone deacetylase inhibitors as anticancer drugs. *Int J Mol Sci*. 2017;18:E1414.
27. Menneveau T, Fabre B, Garrigues L, et al. Mass spectrometry-based absolute quantification of 20S proteasome status for controlled ex vivo expansion of human adipose-derived mesenchymal stromal/stem cells. *Mol Cell Proteomics*. 2019;18:744-759.
28. Nickel W. Pathways of unconventional protein secretion. *Curr Opin Biotechnol*. 2010;21:621-626.
29. Shiba T, Tanaka T, Ida H, et al. Functional evaluation of the pathological significance of MEFV variants using induced pluripotent stem cell-derived macrophages. *J Allergy Clin Immunol*. 2019;144:1438-1441.
30. Takada S, Kambe N, Kawasaki Y, et al. Pluripotent stem cell models of Blau syndrome reveal an IFN- γ -dependent inflammatory response in macrophages. *J Allergy Clin Immunol*. 2018;141:339-349.
31. Kawasaki Y, Oda H, Ito J, et al. Identification of a high-frequency somatic NLRC4 mutation as a cause of autoinflammation by pluripotent cell-based phenotype dissection. *Arthritis Rheumatol*. 2017;69:447-459.
32. Cerri C, Caleo M, Bozzi Y. Chemokines as new inflammatory players in the pathogenesis of epilepsy. *Epilepsy Res*. 2017;136:77-83.
33. Di Luigi L, Corinaldesi C, Colletti M, et al. Phosphodiesterase type 5 inhibitor sildenafil decreases the proinflammatory chemokine CXCL10 in human cardiomyocytes and in subjects with diabetic cardiomyopathy. *Inflammation*. 2016;39:1238-1252.
34. Zoja C, Corna D, Locatelli M, et al. Effects of MCP-1 inhibition by bindarit therapy in a rat model of polycystic kidney disease. *Nephron*. 2015;129:52-61.
35. Lee JH, Kim B, Jin WJ, Kim HH, Ha H, Lee ZH. Pathogenic roles of CXCL10 signaling through CXCR3 and TLR4 in macrophages and T cells: relevance for arthritis. *Arthritis Res Ther*. 2017;19:163.
36. Sasaki-Honda M, Jonouchi T, Arai M, et al. A patient-derived iPSC model revealed oxidative stress increases facioscapulohumeral muscular dystrophy-causative DUX4. *Hum Mol Genet*. 2018;27:4024-4035.
37. Younes A, Berdeja JG, Patel MR, et al. Safety, tolerability, and preliminary activity of CUDC-907, a first-in-class, oral, dual inhibitor of HDAC and PI3K, in patients with relapsed or refractory lymphoma or multiple myeloma: an open-label, dose-escalation, phase 1 trial. *Lancet Oncol*. 2016;17:622-631.
38. Chen Y, Peubez C, Smith V, et al. CUDC-907 blocks multiple pro-survival signals and abrogates microenvironment protection in CLL. *J Cell Mol Med*. 2019;23:340-348.
39. Sanchez GAM, Reinhardt A, Ramsey S, et al. JAK1/2 inhibition with baricitinib in the treatment of autoinflammatory interferonopathies. *J Clin Invest*. 2018;128:3041-3052.
40. Drutskaya MS, Efimov GA, Astrakhantseva IV, Kruglov AA, Nedospasov SA. Making anti-cytokine therapy more selective: studies in mice. *Cytokine*. 2018;101:33-38.
41. Seidel P, Sun Q, Costa L, Lardinois D, Tamm M, Roth M. The MNK-1/eIF4E pathway as a new therapeutic pathway to target inflammation and remodelling in asthma. *Cell Signal*. 2016;28:1555-1562.
42. Dong N, Xu B, Shi H, Tang X. Baicalein inhibits amadori-glycated albumin-induced MCP-1 expression in retinal ganglion cells via a MicroRNA-124-dependent mechanism. *Invest Ophthalmol Vis Sci*. 2015;56:5844-5853.

SUPPORTING INFORMATION

Additional supporting information may be found online in the Supporting Information section at the end of this article.

How to cite this article: Kase N, Terashima M, Ohta A, et al. Pluripotent stem cell-based screening identifies CUDC-907 as an effective compound for restoring the in vitro phenotype of Nakajo-Nishimura syndrome. *STEM CELLS Transl Med*. 2021; 10:455-464. <https://doi.org/10.1002/sctm.20-0198>